Reduction and Agglomeration of Supported Metal Clusters Induced by High-Flux X-ray Absorption Spectroscopy Measurements

M. Albrahim, D. Leshchev

To be published in "JOURNAL OF PHYSICAL CHEMISTRY C"

May 2021

DISCLAIMER

Reduction and Agglomeration of Supported Metal Clusters Induced by High Flux X-ray Absorption Spectroscopy Measurements

Malik Albrahim[1, ‡], *Coogan Thompson*[1, ‡], *Denis Leshchev*[2], *Abhijit Shrotri*[3], *Raymond R. Unocic*[4], *Jiyun Hong*[5], *Adam S. Hoffman*[5], *Michael J. Meloni*[6], *Ron C. Runnebaum*[6], *Simon R. Bare*[5], *Eli Stavitski*[2], *Ayman M. Karim*[1*]

1 Department of Chemical Engineering, Virginia Polytechnic Institute and State University, Blacksburg, Virginia 24060, United States

2 National Synchrotron Light Source II, Brookhaven National Laboratory, Upton, New York 11973, United States

3 Institute for Catalysis, Hokkaido University, Kita ku, Sapporo, Hokkaido 001-0021, Japan

4 Center for Nanophase Materials Sciences, Oak Ridge National Laboratory, Oak Ridge, Tennessee 37831, United States

5 Stanford Synchrotron Radiation Lightsource, SLAC National Accelerator Laboratory, Menlo Park, California 94025, United States

6 Department of Chemical Engineering and Materials Science, University of California, Davis, California 95616, United States

‡These authors contributed equally

KEYWORDS X-ray absorption spectroscopy, in-situ characterization, supported metal nanoparticles, beam effects, catalyst

ABSTRACT: Supported metal clusters are widely used in catalysis for many important reactions. To understand the catalytic properties, *in-situ*/*operando* characterization techniques, such as X-ray absorption spectroscopy, provide essential details about the size, shape and chemical composition of the cluster and the nature of the active sites. New generation synchrotrons combined with focusing beamlines provide high flux density X-rays for improved detection sensitivity as well as higher time- and spatial- resolution. Understanding the effects of a high flux density X-ray beam on the catalyst during the actual measurement, whether XAS or other synchrotron-based techniques, is crucial. This is especially important for *in-situ* and *operando* studies where both the high flux density and reaction conditions can affect the catalyst structure. In this work we investigated the effect of the flux density on rhodium clusters supported on Al_2O_3 at two different beamlines: National Synchrotron Light Source II beamline 08-ID and Stanford Synchrotron Radiation Light Source beamline 4-1. We show that the higher flux density at beamline 08-ID causes reduction of highly dispersed RhO_x/Al_2O_3 catalyst even at room temperature. Additionally, exposure to the higher flux density X-rays at beamline 08-ID during *in-situ* reduction results in significant agglomeration of the Rh clusters. The final size of Rh nanoparticles reduced at 310 °C is equivalent to particles formed after reduction at 600-650 °C in the absence of the beam. Significant beam induced reduction and agglomeration is also shown for Ni supported on beta zeolite during *in-situ* reduction at an intermediate flux density beamline 9-3 at SSRL, indicating that beam induced changes of heterogeneous catalysts could be common at intermediate and high flux density beamlines. We provide precautions and recommendations to detect and minimize beam damage during *in-situ*/*operando* X-ray absorption spectroscopy measurements.

1. INTRODUCTION

Supported metal nanoparticles are widely used to catalyze many chemical transformations. The size, shape and composition strongly affect the nanoparticles' catalytic properties making their characterization, especially *in-situ* and *operando*, essential to develop a more fundamental understanding of catalysis. Advances in imaging and spectroscopy techniques have led to an improved fundamental understanding of the important relationships between the catalytic properties and the structure of the metal clusters/nanoparticles[1]. Experimental techniques such as scanning/transmission electron microscopy (S/TEM) and X-ray absorption spectroscopy (XAS) are used to determine a catalyst's structure, elemental composition and oxidation state through a combination of imaging and spectroscopy. When performing these experiments the catalyst is exposed to both high energy and high dose electron and X-ray beams, which may have the deleterious effect of altering the catalyst structure.

S/TEM imaging is an inherently high spatial resolution imaging technique that can be combined with spectroscopy (energy dispersive X-ray spectroscopy and electron energy loss spectroscopy). The electron beam can induce radiation damage within the specimen which is determined by electron energy (or accelerating voltage) dose used during characterization. For example, it has been reported that a 400 keV electron beam causes small metal clusters, such as platinum and rhodium supported on silica and carbon, to agglomerate into large particles[2-3]. Moreover, nanocrystalline silver particles were observed to grow rapidly (from 15 nm to 2 μm) when exposed to electron beam irradiation [4]. Furthermore, intensive research confirmed the effect of the electron beam from transmission microscopy on supported gold clusters which cause rearrangement, reconstruction and agglomeration to form larger particles[5-6]. Due to these undesirable beams induced effects, new techniques are currently being developed to image beam-sensitive materials: lower keV, lower dose and cryo-EM imaging conditions[7-10].

For heterogeneous catalysts, X-ray beams used for XAS have not typically been associated with causing damage similar to that observed in electron microscopy. As the demand for *in-situ* and *operando* measurements increases along with the need for higher temporal resolution and lower detection limits, beamlines with higher flux (upwards of 10^{12} photons/s) have been increasingly used for XAS measurements of heterogeneous catalysts. A higher flux allows for the detection of low concentration species and observing fast structural changes under *in-situ/operando* conditions. However, a higher X-ray flux, especially when focused to a small area of the sample (i.e. high flux density) can lead to undesirable structure and chemical changes that lead to the appearance of intermediates and structures not actually present during catalysis under the same conditions. Such X-ray induced changes are common and well documented for biological samples and homogeneous catalysts[11-12]. For instance, X-rays have been shown to induce reduction of metal complexes in solution[12-14] as well as nucleation, growth and agglomeration of nanoparticles[15-18]. Similarly, surface grafted Cu^{II} organometallics on SiO_2 and Al_2O_3 were easily reduced to Cu^{I} in a high flux density X-ray beam while Cu^{II} was stable in a non-focused beam (low flux density)[19]. However, while structural and chemical changes induced by high energy electron beams are well documented in S/TEM for heterogeneous catalysts; those effects have only been recently shown for XAS[19]. As the development of higher flux beamlines continues (e.g. so-called diffraction-limited 4th generation synchrotrons), beam effects are likely to become more common rather than being the exception. Unfortunately, most XAS studies of heterogeneous catalysts do not systematically check for beam effects or rarely report them. Therefore, a thorough study/analysis of the extent of beam effects on supported metal nanoparticles is needed to provide an understanding of the damage that might result during *in-situ/operando* XAS measurements at high flux X-ray beamlines.

In this work we have studied the effect of X-ray flux density on the catalyst structure at two different beamlines; a wiggler side station (SSRL BL 4-1) and a damping wiggler station with a higher flux density (NSLS-II BL 08-ID). We support these studies with electron microscopy and H_2 chemisorption. Rhodium supported on alumina was used as a test case since Rh/Al_2O_3 is a well-known catalyst for several important industrial applications, such as three-way catalyst used in automotive catalytic converters, which also has been extensively studied spectroscopically in the past few decades. We found that Rh clusters are very sensitive when exposed to a high X-ray flux density which leads to significant reduction and agglomeration. Using low X-ray flux density ($\sim 10^{10}$ photons/sec/mm^2) during *in-situ* measurements at SSRL BL 4-1, the Rh clusters remain small and the Rh-Rh coordination was consistent with the size obtained from *ex-situ* microscopy. However, using a higher X-ray flux density ($\sim 10^{12}$ photons/sec/mm^2) at NSLS-II BL 08-ID under otherwise similar *in-situ* conditions, the Rh-Rh coordination number increased and became similar to the coordination number for reduction at much higher temperature. The beam induced reduction and agglomeration appear to be more common than previously known. *In-situ* reduction of Ni supported on beta zeolite at an intermediate flux density beamline (SSRL BL 9-3, $\sim 10^{11}$ photons/sec/mm^2) resulted in significant reduction and agglomeration of Ni compared to measurements without beam exposure during reduction. The results indicate that *in-situ/operando* catalyst studies using high flux beamlines need to be carefully designed in order to eliminate/reduce beam damage.

2. EXPERIMENTAL METHODS

2.1 Synthesis and pretreatment

The Rh/Al_2O_3 catalyst with a nominal loading of 0.5 wt% was prepared by strong electrostatic adsorption. The γ-Al_2O3 support (BET surface area 220 m^2/g) was obtained by calcining Boehmite (CATAPAL B from Sasol) at 600 °C for 3 hours before catalyst synthesis. Two grams of γ-Al_2O_3 support was added to 1 L of deionized water at room temperature while stirring (600 rpm). A 300 μL solution of 37 wt% HCl was slowly added to adjust the pH to 3. A Rh solution (20 mL) was prepared by dissolving about 0.01 g of $RhCl_3 \cdot xH_2O$ (Sigma Aldrich 450286, Lot # MKCH3679) in deionized water and a suitable amount of HCl to maintain the pH at 3. The Rh solution was then added to the 1 L Al_2O_3 solution at room temperature while stirring at 600 rpm for 4 hours. The solution was then filtered to separate the solid (catalyst) from the liquid. The catalyst was dried overnight at 80 °C and for 1 hour at 100 °C for 1 hour then calcined at 450 °C with ramp rate of 5 °C/min and held at 450 °C for 4 hours. The actual Rh loading was found to be 0.3 wt% by measuring the Rh concentration in the initial and filtered solutions using inductively coupled plasma atomic emission spectroscopy (ICP-AES). All the reported results were obtained using the same batch of the catalyst to eliminate any possible variations between batches. The catalyst pretreatment was identical for all the experiments and started with an oxidation step in 20% O_2 (99.999% Airgas) balanced with He (99.999% Airgas) at 310 °C (10 °C/min) for 30 min then the catalyst was reduced in 20% H_2 (99.999% Airgas) balanced with He (99.999% Airgas) at 310 °C or 650 °C for 2 hours. The total flowrate was 50 sccm during the pretreatment.

NH_4-[Al]-Beta (Si/Al = 19, Zeolyst CP814C) was dealuminated by mixing NH_4-[Al]-Beta in 13 M HNO_3 for 16 h at 80°C. After dealumination the zeolite was washed with water and then calcined at 500 °C in 10% O_2 for 6 hours, with a hold for 1 hour at 120 °C and ramp rate of

2 °C/min then transferred to an Ar filled glovebox. Ni was deposited by mixing [DeAl]-Beta with Ni(acac)$_2$ (STREM Chemicals) in dried, de-oxygenated n-pentane for 24 hours on a Schlenk line to exclude moisture and O_2. The solvent was then evacuated for 24 hours and the resulting powder was calcined at 600 °C in 10% O_2 for 6 hours, with a 1 hour hold at 120 °C with a ramp rate of 2 °C/min.

2.3 X-ray absorption spectroscopy

The *in-situ* X-ray absorption spectroscopy experiments were performed at the Stanford Synchrotron Radiation Light Source (SSRL) beamline 4-1 (BL 4-1), beamline 9-3 (BL 9-3) and at the National Synchrotron Light Source II (NSLS-II) Inner Shell Spectroscopy (ISS) beamline 08-ID (BL 08-ID). A comparison of the flux and beam size of the beamlines is summarized in Table 1. Details of both beamlines and flow cells used for the measurements are described below.

SSRL BL 4-1 is a 20-pole, 2 - Tesla wiggler side station with vertically collimating mirror. The photon flux is nominally reported to be $2x10^{12}$ photon/s[20]. The flux was measured directly with the Ar ion chamber in order to estimate the flux at the Rh K-edge (23,220 eV). Using the Si [220], φ=0, the measured flux for the beam size used in the experiments (0.25 mm × 4 mm, vertical × horizontal) was $3.2x10^{10}$ photons/s. The catalyst was loaded into a 2.8 mm i.d. (3.0 mm o.d.) quartz tube with a bed length of 10 mm (approximately 30 mg). Two coil heaters approximately 2 mm, one above and the other below, were used to heat the catalyst. Kapton film was put around the setup in order to create a layer of stagnant air for insulation. The temperature inside the reactor was measured via a thermocouple inserted through the reactor tube immediately downstream of the catalyst, only being separated by a thin layer of quartz wool. The reactor has been more thoroughly described in previous work[21].

SSRL BL 9-3 is a 16-pole, 2-Tesla Wiggler, 2 mrad acceptance, with vertically collimating M0 mirror and cylindrically bent Rh coated M1 focusing mirror. The flux is nominally reported to be 2x10^{12} photon/s. The flux was measured directly with a nitrogen filled ion chamber at the Ni K-edge (8400 eV). Using the Si [220], φ=0, the measured flux for the beam size used in the experiments (1.0 mm × 3 mm, vertical × horizontal) was 3.22x10^{11} photons/s (flux density of 1.1x10^{11} photons/s/mm^2). The catalyst was loaded into a 3.0 mm o.d. Kapton tube with a bed length of 10 mm (approximately 40 mg). The experiment was conducted using the same reactor as at BL 4-1, above.

NSLS-II BL 08-ID has a damping wiggler source that provides high flux photon (10^{14} photon/s at 10 keV at full accelerator current) with a 1 mm × 1 mm spot size[22]. The ion chamber response was calibrated using SYDOR diamond detector[23], and at Rh edge the flux is 4x10^{12} photons/s. 100 mg of catalyst was loaded into a custom built 4 mm i.d. glassy carbon tube. An approximately 1”x3”x6” stainless steel block with a vertical bore for the reactor and horizontal rectangular bore through the side and surrounded by approximately 1” ceramic insulation was used as a reactor. The temperature inside the reactor was measured via a thermocouple inserted through the reactor tube immediately downstream of the catalyst, only being separated by a thin layer of quartz wool. The reactor has been more thoroughly described in previous work[24].

Table 1: Details of the beamlines at SSRL and NSLS-II.

BEAMLINE	**SSRL BL 4-1** **WIGGLER SIDE STATION**	**NSLS-II BL 08-ID** **DAMPING WIGGLER STATION**	**SSRL BL 9-3** **2-TESLA WIGGLER**
FLUX at 23,220 eV (photons/s)	3.2×10^{10}	4×10^{12}	$3.22\times10^{11*}$
BEAM SIZE (mm × mm)	0.25×4	1×1	1×3
FLUX DENSITY (photons/s/mm^2)	3.2×10^{10}	4×10^{12}	1.1×10^{11}

* Flux measured at 8,400 eV.

Two experiments for the Rh/Al_2O_3 catalyst were conducted at each beamline, SSRL BL 4-1 and NSLS-II BL 08-ID. The experimental conditions are summarized in Table 2 and described in more details next. At SSRL BL 4-1 for the 310 °C reduced catalyst, EXAFS scans were taken of the fresh, calcined sample. The sample was then oxidized in 16% O_2 (balance He) for 10 minutes at 310 °C (ramp rate of 20 °C/min up and 100 °C/min down). The sample was then reduced in 20% H_2 (balance He) for 2 hours at 310 °C (ramp rate of 10 °C/min up and 100 °C/min down). During the reduction, the catalyst was exposed to the beam. For the 650 °C reduced catalyst, the sample was already reduced *ex-situ* at 650 °C then re-reduced *in-situ* in 20% H_2 (balance He) for 45 minutes at 650 °C (ramp rate of 10 °C/min up and 100 °C/min down). During the reduction, the catalyst was exposed to the beam.

At NSLS-II BL 08-ID, for the 310 °C reduced catalyst, EXAFS scans were taken of the fresh, calcined sample. The sample was then oxidized in 20% O_2 (balance He) for 30 minutes at 310 °C (ramp rate of 10 °C/min up and ~10 °C/min down limited by convective cooling using a fan). EXAFS scans were taken of the sample. The sample was then reduced in 20% H_2 (balance He) for

1 hour at 310 °C (ramp rate of 10 °C/min up and ~10 °C/min down limited by convective cooling). During the reduction, the catalyst was exposed to the beam. After reduction, EXAFS scans were taken of the sample in H_2. For the second experiment, EXAFS scans were taken of the fresh, calcined sample. The sample was then oxidized in 20% O_2 (balance He) for 10 minutes at 200 °C (ramp rate of 10 °C/min up and ~10 °C/min down limited by convective cooling). EXAFS scans were taken of the sample. The sample was then reduced in 20% H_2 (balance He) for 1 hour at 200 °C (ramp rate of 10 °C/min up and ~5 °C/min down limited by convective cooling). During the reduction, the catalyst was not exposed to the beam. After reduction EXAFS scans were taken of the sample in H_2.

Table 2: Summary of the *in-situ* experimental conditions used for the 0.3 wt% Rh/Al_2O_3 catalyst. At both beamlines, ultra-high purity (99.999%) O_2, H_2, CO, and He were blended to get the gas concentrations mentioned using a mass flow control board available at each location.

EXPERIMENT	**SSRL BL 4-1 310 °C**	**SSRL BL 4-1 650 °C**	**NSLS-II BL 08-ID 310 °C**	**NSLS-II BL 08-ID 200 °C**
FLUX at 23,220 eV (photons/s)	3.2×10^{10}	3.2×10^{10}	4×10^{12}	4×10^{12}
BEAM SIZE (mm × mm)	0.25×4	0.25×4	1×1	1×1
OXIDATION	16% O_2 310 °C 10 minutes	None	20% O_2 310 °C 30 minutes	20% O_2 200 °C 10 minutes
REDUCTION	20% H_2 310 °C 2 hours	20% H_2 650 °C 45 minutes	20% H_2 310 °C 1 hour	20% H_2 200 °C 1 hour
BEAM ON DURING REDUCTION	Yes	Yes	Yes	No

The parameters for the respective measurements were: a) Scan time was ~11 minutes and ~40 seconds (including time for the monochromator to reset in between scans) at SSRL and NSLS-II, respectively. b) At both beamlines data were collected in both transmission and fluorescence modes, however only the fluorescence data is used in our analysis. c) A Passivated Implanted Planar Silicon (PIPS) detector mounted at a 90° angle from the beam was used for fluorescence detection at both beamlines. At BL 4-1 transmission data were collected with ionization chambers filled with Ar at 1 atm. While at BL08-ID ionization chambers filled with a mixture of He and N_2 (2 parts He, 5 parts N_2) at 1 atm. These detectors were located upstream of the sample, between the sample and the reference foil, and downstream of the reference foil.

The details of *in-situ* experiments on Ni/beta zeolite at SSRL BL 9-3 are provided in the supporting information.

Data processing and analysis, for the X-ray absorption near edge and the extended X-ray absorption fine structure (XANES and EXAFS), were performed using Athena and Artemis programs of the Demeter data analysis package[25-26]. After the normalization of the absorption coefficient, the smooth atomic background was subtracted using the AUTOBKG code in Athena to obtain $\chi(k)$ (where k is the photoelectron wave number). The theoretical EXAFS signal for Rh-O and Rh-Rh scattering paths were constructed using the FEFF6[27] code using the crystal structure of Rh_2O_3 and Rh metal, respectively. The theoretical EXAFS signals were fitted to the data in r-space using Artemis by varying the coordination numbers of the single scattering paths, the effective scattering lengths, the bond length disorder and the correction to the threshold energy, ΔE_0, for each path; Rh-O and Rh-Rh. S_0^2 (the passive electron reduction factor) was obtained by first analyzing the first shell of the Rh foil spectrum, and the best fit value (0.85±0.04 for data collected at SSRL BL 4-1 and 0.84±0.05 for data collected at NSLS-II BL 08-ID) was fixed for the fit. The k-range used for the Fourier transform of χ(k) was 3-12.5 Å^{-1} (3-14 Å^{-1} for the reduced catalysts) and the r-range for fitting was 1.2-3.1 Å. The best parameters fit using k-weights of 1, 2, and 3 (simultaneously) in Artemis are reported, however, the results were similar to those using only a k-weight of 2. Additionally, the k-range did not have a significant effect on the best fit values of the model fit but did affect their uncertainties.

2.4 Aberration corrected scanning transmission electron microscopy

Aberration-corrected scanning transmission electron microscopy was used to measure the particle size distribution of the 0.3 wt% Rh/Al_2O_3 catalyst after reduction in H_2 at 310 °C and 650 °C. The calcined catalyst was pretreated first in 20 kPa O_2 (balance He at 95 sccm total flowrate) at 310 °C with ramp rate 10 °C/min and held for 1 hour then reduced using H_2 at 20 kPa (balanced with He) at 310 °C with ramp rate 10 °C/min and held for 2 hours. The reduced catalysts were characterized *ex-situ* using an aberration corrected Nion UltraSTEM operating at 100 keV and on an aberration corrected JEOL JEM-ARM200F at an acceleration voltage of 200 kV. We measured the diameter of about 100 particles using the ImageJ software where both the size measurements of the particles and counting the Rh single atoms was done manually[28]. The number, surface and volume average particle sizes (diameter) were calculated as $\sum_i^N \frac{n_i d_i}{n_i}$, $\sum_i^N \frac{n_i d_i^2}{n_i d_i}$ and $\sum_i^N \frac{n_i d_i^3}{n_i d_i^2}$, respectively[29].

2.5 H_2 volumetric chemisorption

Volumetric H_2 chemisorption was carried out using Micromeritics 3Flex surface characterization analyzer. 0.5 g of 0.3 wt% Rh/Al_2O_3 was used for the H_2 volumetric chemisorption. The catalyst (pellet size between 150 µm to 250 µm) was packed in a quartz sample holder. The catalyst was pretreated with an oxidation step at 310 °C and a reduction step at 310 °C or 650 °C. The pretreatment was performed in static mode where the oxidation step start was adding pure O_2 at room temperature and heated up to 310 °C with ramp rate 10 °C/min and held for 30 min followed by evacuation at 310 °C for 30 min. This procedure of adding oxygen for 30 min then evacuation was repeated three times. The sample was then evacuated at 310 °C for 30 mins and cooled to 35 °C. The reduction step started with adding pure H_2 at 35 °C and was then heated up to 310 °C or 650 °C with ramp rate 10 °C/min and held for 30 min followed by an evacuation step at 310 °C or 650 °C for 30 minutes. Adding pure hydrogen and holding for 30 min followed by an evacuation was repeated 4 times for a total time of 2 hours. After the pretreatment, the sample was evacuated at 310 °C or 650 °C for 30 minutes, then cooled at 35 °C while still under vacuum before the H_2 volumetric chemisorption. Two H_2 chemisorption isotherms were performed with an evacuation step between them to remove the physisorbed H_2. The difference between the first and second isotherms was used to calculate the quantity of chemisorbed H_2 and H:Rh ratio.

3. RESULTS AND DISCUSSION

3.1 Rh size distribution after *ex-situ* reduction and H_2 volumetric chemisorption

Figure 1a shows HAADF-STEM image for the 0.3 wt% Rh/Al_2O_3 catalyst after reduction at 310 °C. The image shows mostly Rh subnanometer clusters and small nanoparticles with a narrow size distribution ranging from 0.5-1.2 nm along with a few Rh single atoms as shown in Figure 1b. The number-average, surface-average and volume average-diameters were calculated to be 0.8, 0.85 and 0.9 nm, respectively. The small size is due to the low Rh loading and low reduction temperature which is also consistent with previous reports that Rh/Al_2O_3 prepared using $RhCl_3$ as a precursor can form uniform particles (ranging from 0.3 nm to 1.7 nm) even with reduction temperatures of 500 °C[30]. On the other hand, when the catalyst was reduced at 650 °C, the particle size increased, as shown in the STEM image in Figure 1c and the size distribution in Figure 1d. The number-average, surface-average and volume average diameters were calculated to be 1.4, 1.5 and 1.6 nm, respectively. The H:Rh ratio from H_2 chemisorption on the 0.3 wt% Rh/Al_2O_3 catalyst reduced at 310 and 650 °C was 0.85 and 0.62, respectively which are consistent with the sizes measured from STEM.

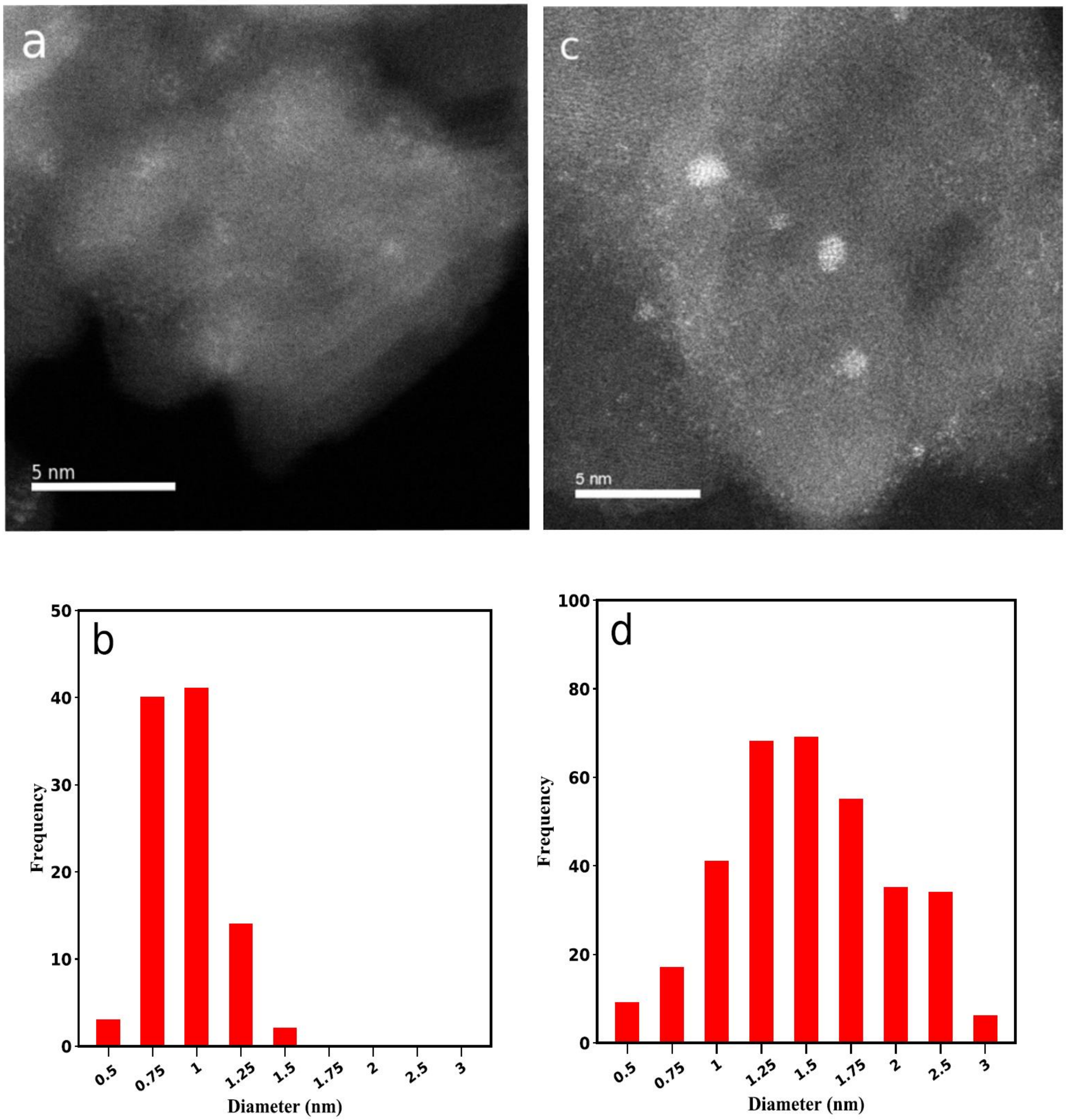

Figure 1: (a) and (b) STEM images for 0.3 wt% Rh/Al_2O_3 after reduction at 310 °C and 650 °C. (c) and (d) are the particle size distributions of the reduced catalysts at 310 °C (created by measuring the diameter of 100 particles from 20 different images) and 650 °C (created by measuring the diameter of 320 particles from over 40 images)

3.2 Effect of the X-ray beam on Rh oxidation state at room temperature

Before performing *in-situ* reduction experiments at elevated temperatures, we started by investigating the effect of the X-ray flux density on the state of the calcined Rh/Al_2O_3 catalyst at room temperature. The XANES and EXAFS spectra for the calcined 0.3 wt% Rh/Al_2O_3 were similar at both beamlines, and the Rh-O coordination number was 6.5±1.5 (Table S1). No changes in the spectra were observed during the 10-30 minutes oxidation step at 310 °C at both beamlines (Figure S1). Figures 2a and 2b show time resolved Rh K-edge XANES of the calcined 0.3 wt% Rh/Al_2O_3 catalyst at room temperature under 20% H_2 (balance He) for experiments performed at SSRL BL 4-1 and NSLS-II BL 08-ID, respectively. For the SSRL BL 4-1 experiment, no changes were observed as shown in Figure 2a. On the other hand, the higher flux density at NSLS-II BL 08-ID resulted in an observable decrease of the white line intensity over time under H_2 as shown in Figure 2b. The decrease in the white line intensity and the formation of isosbestic points at 23,255 and 23,285 eV are associated with partial reduction of rhodium oxide (Rh^{+3}) into Rh metal (Rh^0)[30-31]. A linear combination fit of the XANES spectra using Rh foil and the calcined catalyst as standards show that Rh is ~29% reduced at room temperature after 6 min exposure to the beam at NSLS-II BL 08-ID. In addition, the EXAFS spectra in Figures 2c and 2d show a decrease in the intensity of the Rh-O peak (at ~1.5 Å) and the corresponding Rh-O coordination number decreased from 6.5±1.5 in O_2 to 5.0±1.5 after 6 minutes in H_2 (Table S1). The EXAFS results indicate a partial reduction of Rh at room temperature which is consistent with the XANES results in Figure 2b. It is well known that reduction of highly dispersed RhO_x supported on Al_2O_3 does not start until ~150 °C[32-33]. Our temperature programmed reduction results (Figure S2) showed that a temperature of 100-120 °C is required to start the reduction of Rh in the calcined 0.3 wt% Rh/Al_2O_3 catalyst. At SSRL BL 4-1, the beam did not affect the oxidation state of Rh at room temperature regardless of gas environment (H_2 or O_2). Therefore, the partial reduction of Rh^{3+} in H_2 at NSLS-II BL 08-ID is indicative of a beam effect caused by the high flux density even within 6 min of exposure to the beam.

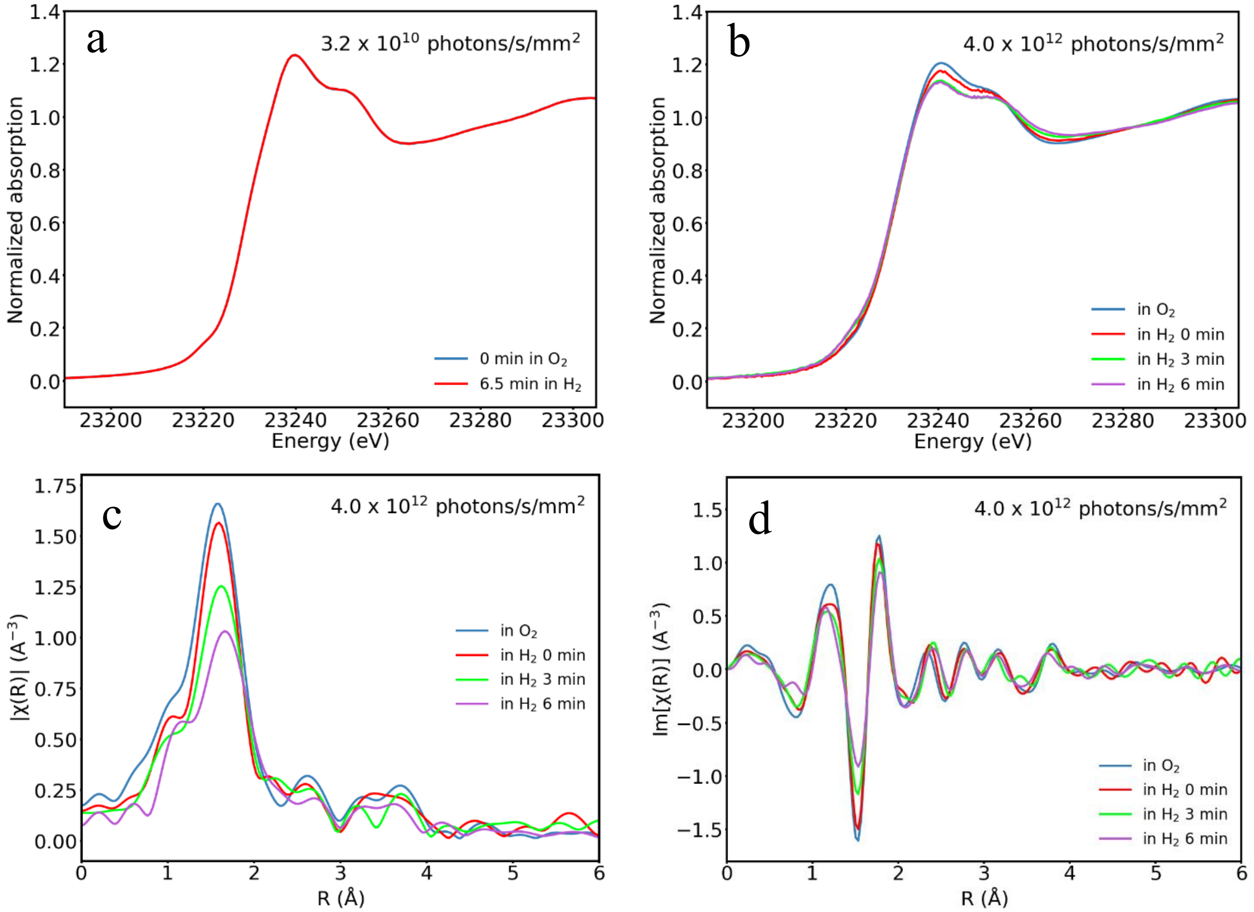

Figure 2: Rh K-edge X-ray absorption spectroscopy for 0.3 wt% Rh/Al_2O_3 at room temperature under a flow of 20% H_2 (balanced with He). (a) XANES at SSRL BL 4-1 (3.2×10^{10} photons/s/mm^2), (b) XANES at NSLS-II BL 08-ID (4×10^{12} photons/s/mm^2), (c) EXAFS magnitude and (d) imaginary parts of the Fourier transformed k2-weighted χ(k) data, Δk = 3-13 Å^{-1} for the experiment at NSLS-II BL 08-ID (4×10^{12} photons/s/mm^2).

3.4 Effect of the X-ray beam on average Rh cluster size resulting from *in-situ* reduction

In addition to the observed changes at room temperature as a result of the high beam density at NSLS-II 08-ID, we also observed significant changes during and after reduction compared to the same experiment performed at SSRL BL 4-1. Linear combination fitting of the *in-situ* XANES during reduction (Figure S3) shows that Rh is significantly more reduced at the same temperature at NSLS-II BL 08-ID. Figure 3 shows a comparison of the EXAFS spectra at SSRL BL 4-1 and NSLS-II 08-ID after reduction at 310 °C for 2 hours. It can be seen that there is significantly higher intensity for the Rh-Rh scattering peak (at ~2.6 Å) from the NSLS-II BL 08-ID experiment compared to that at SSRL BL 4-1, indicating a larger average Rh cluster size. Indeed, the EXAFS modeling results (Table 3) show that the Rh-Rh coordination numbers were 4.0±0.5 and 6.2±0.8 at SSRL BL 4-1 and NSLS-II 08-ID, respectively. Assuming hemispherical shaped clusters[34], the coordination numbers of 4.0±0.5 and 6.2±0.8 correspond to an average diameter of ~0.5 nm and 1.0 nm at SSRL BL 4-1 and NSLS-II BL 08-ID, respectively. The number-average diameter from HAADF-STEM after reduction at 310 °C was 0.8 nm which is larger than the estimated size from EXAFS at SSRL BL 4-1. The presence of Rh single atoms in the catalyst after reduction at 310 °C, as shown in Figure 1, is likely the cause of the lower than expected Rh-Rh coordination number. The Rh-O coordination number of 0.4 is also consistent with Rh single atoms and Rh atoms in small clusters, which are coordinated with oxygens from the support. In principle, if the percentage of single atoms is known, the Rh-Rh coordination can be corrected to reflect the clusters only. However, due to the low number of single atoms and clusters in the HAADF-STEM images, the estimated percentage of single atoms (5%) is likely underestimated and could not be used to calculate the actual Rh-Rh coordination number for the nanoparticles. For the experiment at NSLS-II BL 08-ID, including Rh-O scattering path in the EXAFS model was not necessary for the best fit, which is consistent with the larger Rh size. It is clear from the *in-situ* XANES and EXAFS results that the higher flux density at NSLS-II BL 08-ID compared to SSRL BL 4-1 causes higher extent of reduction at lower temperature and agglomeration of Rh during reduction. This can be seen from the *in-situ* XANES spectra at 200 °C in Figure S4 and from the results of the linear combination fits of the *in-situ* XANES spectra in Figure S3, which shows more reduction at all temperatures at NSLS-II BL 08-ID than at SSRL BL 4-1. Furthermore, Figure S5 compares the *in-situ* XANES spectra at 100 and 200 °C to the spectrum collected after reduction at 200 °C without exposure to the beam. The results in Figure S5 show that more reduction occurs in the beam at NSLS-II BL 08-ID while heating to 200 °C than after 2 hours reduction at 200 °C without exposure to the beam. What is remarkable is that the EXAFS results at NSLS-II BL 08-ID for reduction at 310 °C were similar to those from SSRL BL 4-1 after reduction at 650 °C as shown in Table 3 and Figure 3. This is very surprising and shows the large extent a high flux beam can affect a catalyst during *in-situ* experiments.

Table 3: Summary of the EXAFS modeling parameters for 0.3 wt% Rh/Al_2O_3 after *in-situ* reduction at SSRL BL 4-1 and NSLS-II BL 08-ID. A comparison between the fits and data is provided in Figure S6.

Beamline	SSRL BL 4-1	SSRL BL 4-1	SSRL BL 4-1	NSLS-II BL 08-ID
Flux (photon/s)	3.2×10^{10}	3.2×10^{10}	3.2×10^{10}	4×10^{12}
Beam size (height × width, mm × mm)	0.25×4	0.25×4	0.25×4	1×1
Flux density (photon/s/mm^2)	3.2×10^{10}	3.2×10^{10}	3.2×10^{10}	4×10^{12}
Reduction temperature (°C)	310	650[a]	650	310
N_{Rh-Rh}	4.0±0.5	5.3±0.6[a]	5.6±0.4	6.2±0.8
N_{Rh-O}	0.4±0.2	0.2±0.3		-
R_{Rh-Rh} (Å)	2.655±0.008	2.663±0.008	2.662±0.005	2.677±0.005
R_{Rh-O} (Å)	2.11±0.04	2.16±0.05		-
$\sigma^2_{Rh-Rh} \times 10^3$ (Å^2)	12±1	8±1	9±1	6±1
$\sigma^2_{Rh-O} \times 10^3$ (Å^2)	3±5	1±8		
$\Delta E_{0\ Rh-Rh}$ (eV)	1.5±0.8	4.0±0.7	3.6±0.6	2.7±0.9
$\Delta E_{0\ Rh-O}$(eV)	6±6	10[a]		
Reduced χ^2	281	310	277	1482
R-factor	0.0031	0.005	0.006	0.010

[a] Including a Rh-O scattering path for the Rh/Al_2O_3 catalyst reduced at 650 °C had a negligible effect on the fit and especially the Rh-Rh coordination number.

[b] fixed during the fit

Notation: N, coordination number of absorber-backscatterer pair; R, radial absorber-backscatterer distance; □^{1}, the mean square displacement of the half-path length and represents the stiffness of the bond for a single scattering path, ┤‖E_0, correction to the threshold energy.

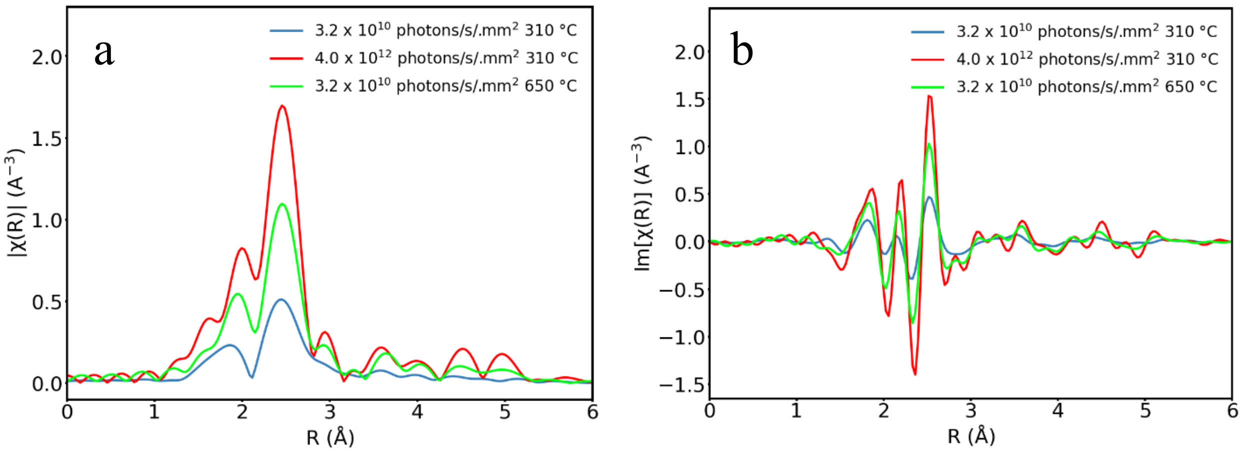

Figure 3: Rh K-edge X-ray absorption spectroscopy for 0.3 wt% Rh/Al_2O_3 after reduction at 310 and 650 °C. The spectra are labelled by the beamline flux density, NSLS-II BL 08-ID (4×10^{12} photons/s/mm^2) and SSRL BL 4-1 (3.2×10^{10} photons/s/mm^2). The spectra were collected in H_2 at room temperature. (a) EXAFS magnitude and (d) imaginary part of the Fourier transformed k^2-weighted χ(k) data, Δk = 3-13 Å^{-1}. k-space data is shown in Figure S7.

3.5 Effect of the X-ray beam at NSLS-II BL 08-ID on an *ex-situ* reduced catalyst

In-situ/*operando* characterization of a catalyst provides invaluable information to help identify the structure/active sites and to understand the reaction mechanism[35-37]. However, *in-situ*/*operando* X-ray absorption measurements can take hours (reduction, different reaction conditions, etc.) to perform while the catalyst is exposed to the X-ray beam. The long exposure to the X-ray beam can have a significant effect on the catalyst structure as seen from the results in Figure 3 and Table 3. Therefore, we also investigated the effect of the high flux density at NSLS-II BL 08-ID on the 0.3 wt% Rh/Al_2O_3 catalyst after *ex-situ* reduction at 200 °C, i.e. without exposure to the X-ray beam to avoid any beam damage during reduction. We chose a reduction temperature of 200 °C because Rh would be mostly present as isolated single atoms with some small clusters which are likely more sensitive to the beam. The time resolved XANES spectra in Figures 4a,b show a decrease in the Rh while line intensity from about 0.5 min to 104 min accompanied by an increase in the Rh-Rh peak intensity in the corresponding EXAFS spectra (Figures 4c,d) and an increase in the Rh-Rh coordination number from 0.4 to 1.6 (Table S2). The absence of isosbestic points in the XANES spectra (Figures 4a,b) suggests the formation of an intermediate species between Rh single atoms and reduced Rh clusters[38-39]. We note that the effect of the beam on the catalyst reduced at 200 °C was observed after longer exposure (10-100 min, Figure 4) compared to the calcined sample (2-6 min in Figure 1b) indicating a synergistic effect of the temperature, H_2 (gas environment), and the X-ray beam.

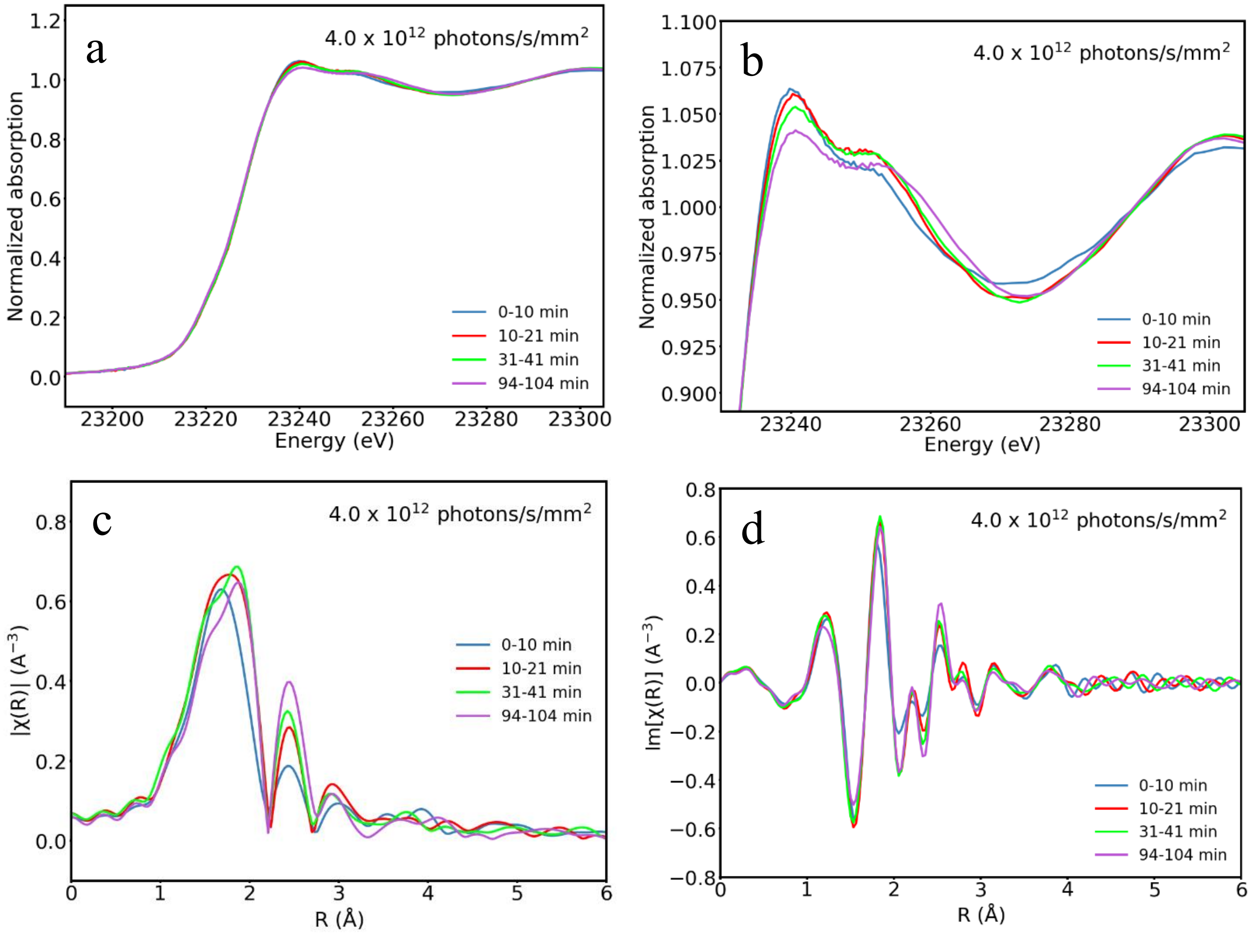

Figure 4: Rh K-edge X-ray absorption spectroscopy for 0.3 wt% Rh/Al_2O_3 after reduction at 200 °C at NSLS-II BL 08-ID (4 × 10^{12} photons/s/mm^2). (a), (b) XANES, (c) EXAFS magnitude and (d)

imaginary part of the transformed k^2-weighted $\chi(k)$ data, $\Delta k = 3\text{-}12$ Å^{-1}. The catalyst was not exposed to the beam during reduction. All spectra were collected at room temperature.

Despite the advantages of using high flux X-ray beams for *in-situ* measurements on understanding the effect of reduction and reaction conditions on the catalyst structure, the beam can cause undesirable changes that can lead to misleading results. We show that a metal supported catalyst such as Rh/Al_2O_3 can be easily damaged by high-flux density X-rays during *in-situ* XAS measurements. We note that the flux density needed to cause damage to a catalyst is relative and likely metal and support dependent. For example, for Ni supported on zeolite beta, we observed significant reduction and agglomeration by exposure to the beam during *in-situ* reduction (Figure S8) at an intermediate flux density beamline, SSRL BL 9-3 (1.1×10^{11} photons/s/mm^2). The linear combination fits of the XANES spectra (Figure S8) show that exposure to the beam resulted in much higher extent of reduction (~96%) and formation of Ni nanoparticles compared with ~57% reduction for the portion of the sample not exposed to the beam.

It has been proposed that the mechanism for X-ray-induced reduction of metal complexes in solution is caused by solvated electrons produced by H_2O radiolysis and/or caused by ligand desorption[15, 41-42]. For Rh/Al_2O_3, as heterogenous catalyst in a gas environment, the mechanism of X-ray beam-induced reduction and agglomeration could be due to local heating effect or by secondary electron generated by the interaction of the X-rays with the rhodium atoms. Pagliero, et al.[43] showed that 17 keV X-ray nanobeam with flux density of 1.4×10^{19} photons/s/mm^2 (photon flux 1.9×10^{11} s^{-1} and beam size 117 nm × 116 nm), caused changes in the oxygen doping levels in $Bi_2Sr_2CaCu_2O_{8+\delta}$ (Bi-2212) superconducting single crystal. Using a finite element model, they found that radiation heating by the final phonon-assisted decay of the power delivered to the crystal by the X-ray nanobeam only increased temperature by a maximum of ~23.6 K. They suggested that the oxygen doping change in the Bi-2212 superconductor is due to secondary electrons[43]. In addition, other reports also confirm that the X-ray-induced effects due to heating the sample are unlikely unless very high flux densities~10^{22} photons/s/mm^2 are used[44]. In our Rh/Al_2O_3 experiments, the beam-induced reduction and agglomeration at NSLS-II BL 08-ID was equivalent to overheating the sample by ~350 °C (Figure 3). However, the flux density at NSLS-II BL 08-ID of 4×10^{12} photons/s/mm^2 is orders of magnitude lower than the values needed to cause significant heating. Therefore, we propose that the main source of X-ray beam-induced reduction and agglomeration of Rh is likely secondary electrons. Specifically, secondary electrons on the metal surface can generate reactive adsorbed species (e.g. O_2^-) which can lead to oxidation of the metal[45] or degradation of ligands[46]. For Rh/Al_2O_3, the X-ray beam-induced reduction/agglomeration could have a similar mechanism involving secondary electrons. Rh is initially oxidized (RhO_x), but in the presence of the X-ray beam the oxygen bound to RhO_x is activated by secondary electrons. In a H_2 atmosphere the activated oxygen on the surface of RhOx reacts with H_2 resulting in reduction of Rh. The higher X-ray flux density at NSLS-II BL 08-ID compared with SSRL BL 4-1 will result in a higher number of secondary electrons and thus a faster reduction rate even at room temperature as seen in our work. Additionally, it is well known that addition of moisture accelerates mobility and the sintering of Rh/Al_2O_3[47]. The activation of water molecules (water produced from the reduction of RhO_x) and possibly neighboring hydroxyl groups on the support by secondary electrons could be the reason for the higher mobility of Rh and formation of larger clusters by the high flux density at NSLS-II BL 08-ID. This proposed mechanism is consistent with the stability of Rh in the beam in an O_2 atmosphere. In the event of activation of O in RhO_x by secondary electrons, the presence of O_2 in the gas phase will likely re-oxidize Rh and keep it dispersed as RhO_x, consistent with our results in O_2 atmosphere.

Our work shows that X-ray beam induced changes to heterogeneous catalysts might be more common, especially during *in-situ/operando* experiments. Furthermore, the results illustrate the importance and need for determining whether the X-ray beam influences the measured XAS data before reporting the results. We fully acknowledge the time pressures of performing experiments at a synchrotron, where a researcher typically only gains access for a few days every few months. However, our work reported here makes it clear that it is critical to take the time necessary to ensure that the reported data are not impacted by the measurement itself. At a minimum, we recommend that all heterogeneous catalyst samples, especially those measured *in-situ* and/or *operando*, be tested for beam effects by moving the beam to a different spot (see for example Figures S8 and S9). To avoid areas in the sample where the scattered beam would have generated secondary electrons and possibly resulted in beam damage, we estimate that a distance of 1-2 beam sizes would be needed between the new and previous spots. Furthermore, our results and other recent work[19] show the importance of minimizing the exposure time of heterogeneous catalysts to high flux density X-rays. The results highlight the need for fast, hard shutters, more sensitive/faster detectors and methods for minimizing background signal other than the metal of interest to minimize the X-ray dose on the catalyst. We anticipate that improved detection will not only allow higher flux beamlines to be used for lower concentration samples and detection of fast structural changes during *in-situ*/*operando* experiments without causing beam damage, it will also enable the use of low X-ray flux density beamlines for a larger range of *in-situ*/*operando* experiments.

CONCLUSIONS

We investigated the effect of X-ray flux density on the structure of a Rh/Al_2O_3 catalyst consisting of highly dispersed Rh. Our results show that higher X-ray flux density can cause reduction of Rh at room temperature and significant agglomeration of Rh during the *in-situ* reduction. The agglomeration caused by exposure to the high flux density X-rays during reduction at 310 °C was similar to increasing the reduction temperature to 650 °C without exposure to the beam. Similar beam effects were observed for Ni/beta zeolite at an intermediate flux density beamline, indicating that beam damage is likely more common and the flux threshold needed is metal/support dependent. The results indicate that experiments at high flux beamlines need to be carefully designed to detect and mitigate beam damage that could adversely affect the structure of the catalyst. Additionally, the results indicate that improving detection to limit exposure to the beam is crucial for long duration *in-situ*/*operando* experiments at intermediate/high flux density beamlines, even for less sensitive catalyst samples.

ASSOCIATED CONTENT

Additional Figures and Tables for XANES, EXAFS and model fits are provided in the supporting information.

AUTHOR INFORMATION

Corresponding Author
*E-mail: amkarim@vt.edu

ACKNOWLEDGMENTS

This research was primarily sponsored by the Army Research Office and was accomplished under Grant Number W911NF-19-1-0308. A part of this work was supported by the Cooperative Research Program of Institute for Catalysis, Hokkaido University (20A1004). Support from Nanotechnology Platform Program of the Ministry of Education, Culture, Sports, Science and Technology (MEXT) is also acknowledged. STEM imaging was conducted at the Center for Nanophase Materials Sciences, which is a Department of Energy Office of Science User Facility

(R.R.U.) M.A. acknowledges support by the graduate fellowship sponsored by the Saudi Arabian Cultural Mission (SACM) and University of Hail (UOH). Use of the Stanford Synchrotron Radiation Light Source (SSRL, beamline 4-1, user proposal 4645), SLAC National Accelerator Laboratory is supported by the U.S. Department of Energy, office of Basic Energy Sciences under Contract No. DE-AC02-76SF00515. Additional support by the Consortium for Operando and Advanced Catalyst Characterization via Electronic Spectroscopy and Structure (Co-ACCESS) at SLAC is acknowledged. Co-ACCESS, is supported by the U.S. Department of Energy, Office of Science, Office of Basic Energy Sciences, Chemical Sciences, Geosciences and Biosciences under Contract DE-AC02-76SF00515. This research used beamline 08-ID (ISS) of the National Synchrotron Light Source II, a U.S. Department of Energy (DOE) Office of Science User Facility operated for the DOE Office of Science by Brookhaven National Laboratory under Contract No. DE-SC0012704.

REFERENCES

1. Chorkendorff, I.; Niemantsverdriet, J. W. *Concepts of Modern Catalysis and Kinetics*; John Wiley & Sons, 2017.
2. Petford-Long, A. K.; Smith, D. J.; Wallenberg, L.; Bovin, J.-O. On the Growth of Small Crystals of Cd, Zn, Pt and Rh During Electron Microscope Observations. *Journal of crystal growth* **1987**, *80*, 218-224.
3. Yoshida, K.; Bright, A.; Tanaka, N. Direct Observation of the Initial Process of Ostwald Ripening Using Spherical Aberration-Corrected Transmission Electron Microscopy. *Journal of electron microscopy* **2012**, *61*, 99-103.
4. Li, Y.; Duan, X.; Qian, Y.; Yang, L.; Liao, H. Nanocrystalline Silver Particles: Synthesis, Agglomeration, and Sputtering Induced by Electron Beam. *Journal of colloid and interface science* **1999**, *209*, 347-349.
5. Wallenberg, L.; Bovin, J.-O.; Schmid, G. On the Crystal Structure of Small Gold Crystals and Large Gold Clusters. *Surface Science* **1985**, *156*, 256-264.
6. Wallenberg, R.; Bovin, J.-O.; Smith, D. J. Atom Hopping on Small Gold Particles Imaged by High-Resolution Electron Microscopy. *Naturwissenschaften* **1985**, *72*, 539-541.
7. Krivanek, O. L.; Chisholm, M. F.; Nicolosi, V.; Pennycook, T. J.; Corbin, G. J.; Dellby, N.; Murfitt, M. F.; Own, C. S.; Szilagyi, Z. S.; Oxley, M. P. Atom-by-Atom Structural and Chemical Analysis by Annular Dark-Field Electron Microscopy. *Nature* **2010**, *464*, 571-574.

8. Zhu, Y.; Ciston, J.; Zheng, B.; Miao, X.; Czarnik, C.; Pan, Y.; Sougrat, R.; Lai, Z.; Hsiung, C.-E.; Yao, K. Unravelling Surface and Interfacial Structures of a Metal–Organic Framework by Transmission Electron Microscopy. *Nature materials* **2017**, *16*, 532-536.
9. Zachman, M. J.; Hachtel, J. A.; Idrobo, J. C.; Chi, M. Emerging Electron Microscopy Techniques for Probing Functional Interfaces in Energy Materials. *Angewandte Chemie* **2020**, *132*, 1400-1412.
10. Bell, D. C.; Mankin, M.; Day, R. W.; Erdman, N. Successful Application of Low Voltage Electron Microscopy to Practical Materials Problems. *Ultramicroscopy* **2014**, *145*, 56-65.
11. Henderson, R. The Potential and Limitations of Neutrons, Electrons and X-Rays for Atomic Resolution Microscopy of Unstained Biological Molecules. *Quarterly reviews of biophysics* **1995**, *28*, 171-193.
12. Mesu, J. G.; Beale, A. M.; De Groot, F. M.; Weckhuysen, B. M. In *Observing the Influence of X-Rays on Aqueous Copper Solutions by in Situ Combined Video/Xafs/Uv-Vis Spectroscopy*, AIP Conference Proceedings, American Institute of Physics: 2007; pp 818-820.
13. Kubin, M.; Kern, J.; Guo, M.; Källman, E.; Mitzner, R.; Yachandra, V. K.; Lundberg, M.; Yano, J.; Wernet, P. X-Ray-Induced Sample Damage at the Mn L-Edge: A Case Study for Soft X-Ray Spectroscopy of Transition Metal Complexes in Solution. *Physical Chemistry Chemical Physics* **2018**, *20*, 16817-16827.
14. Ohkubo, Y.; Nakagawa, T.; Seino, S.; Kugai, J.; Yamamoto, T. A.; Nitani, H.; Niwa, Y. X-Ray-Induced Reduction of Au Ions in an Aqueous Solution in the Presence of Support Materials and in Situ Time-Resolved Xanes Measurements. *Journal of Synchrotron Radiation* **2014**, *21*, 1148-1152.
15. Marignier, J.; Belloni, J.; Delcourt, M.; Chevalier, J. Microaggregates of Non-Noble Metals and Bimetallic Alloys Prepared by Radiation-Induced Reduction. *Nature* **1985**, *317*, 344-345.
16. Higgins, M. C. M.; Clifford, D. M.; Rojas, J. V., Au@ TiO_2 Nanocomposites Synthesized by X-Ray Radiolysis as Potential Radiosensitizers. *Applied Surface Science* **2018**, *427*, 702-710.
17. Walker, C. R.; Pushpavanam, K.; Nair, D. G.; Potta, T.; Sutiyoso, C.; Kodibagkar, V. D.; Sapareto, S.; Chang, J.; Rege, K. Generation of Polypeptide-Templated Gold Nanoparticles Using Ionizing Radiation. *Langmuir* **2013**, *29*, 10166-10173.
18. Feldman, V. I.; Zezin, A. A.; Abramchuk, S. S.; Zezina, E. A. X-Ray Induced Formation of Metal Nanoparticles from Interpolyelectrolyte Complexes with Copper and Silver Ions: The Radiation-Chemical Contrast. *The Journal of Physical Chemistry C* **2013**, *117*, 7286-7293.
19. Newton, M. A.; Knorpp, A. J.; Meyet, J.; Stoian, D.; Nachtegaal, M.; Clark, A. H.;Safonova, O. V.; Emerich, H.; van Beek, W.; Sushkevich, V. L., et al. Unwanted Effects of X-Rays in Surface Grafted Copper(II) Organometallics and Copper Exchanged Zeolites, How They Manifest, and What Can Be Done About Them. *Phys. Chem. Chem. Phys.* **2020**, *22*, 6826-6837.
20. Stanford Synchrotron Radiation Lightsource Experimental Station 4-1. https://www-ssrl.slac.stanford.edu/content/beam-lines/bl4-1 (accessed April 19, 2021).
21. Hoffman, A. S.; Singh, J. A.; Bent, S. F.; Bare, S. R. In Situ Observation of Phase Changes of a Silica-Supported Cobalt Catalyst for the Fischer–Tropsch Process by the Development of a Synchrotron-Compatible in Situ/Operando Powder X-Ray Diffraction Cell. *Journal of Synchrotron Radiation* **2018**, *25*, 1673-1682.

22. Palomino, R. M.; Stavitski, E.; Waluyo, I.; Chen-Wiegart, Y.-c. K.; Abeykoon, M.; Sadowski, J. T.; Rodriguez, J. A.; Frenkel, A. I.; Senanayake, S. D. New in-Situ and Operando Facilities for Catalysis Science at NSLS-II: The Deployment of Real-Time, Chemical, and Structure-Sensitive X-Ray Probes. *Synchrotron Radiation News* **2017**, *30*, 30-37.
23. Sydor Technologies Diamond Beam Position Monitors for X-Ray Beamlines. https://sydortechnologies.com/x-ray-beam-monitors/ (accessed Jan 12, 2021).
24. Karim, A. M.; Howard, C.; Roberts, B.; Kovarik, L.; Zhang, L.; King, D. L.; Wang, Y. In Situ X-Ray Absorption Fine Structure Studies on the Effect of Ph on Pt Electronic Density During Aqueous Phase Reforming of Glycerol. *ACS Catalysis* **2012**, *2*, 2387-2394.
25. Ravel, B.; Newville, M. Athena, Artemis, Hephaestus: Data Analysis for X-Ray Absorption Spectroscopy Using Ifeffit. *Journal of Synchrotron Radiation* **2005**, *12*, 537-541.
26. Newville, M. Exafs Analysis Using Feff and Feffit. *Journal of Synchrotron Radiation* **2001**, *8*, 96-100.
27. Zabinsky, S. I.; Rehr, J. J.; Ankudinov, A.; Albers, R. C.; Eller, M. J. Multiple-Scattering Calculations of X-Ray-Absorption Spectra. *Physical Review B* **1995**, *52*, 2995-3009.
28. Collins, T. J. Imagej for Microscopy. *Biotechniques* **2007**, *43*, S25-S30.
29. Ertl, G.; Knözinger, H.; Weitkamp, J. Handbook of Heterogeneous Catalysis. **1997**.
30. Duarte, R.; Safonova, O.; Krumeich, F.; van Bokhoven, J. A. Atomically Dispersed Rhodium on a Support: The Influence of a Metal Precursor and a Support. *Physical Chemistry Chemical Physics* **2014**, *16*, 26553-26560.
31. Newton, M. A.; Dent, A. J.; Diaz-Moreno, S.; Fiddy, S. G.; Jyoti, B.; Evans, J. Rapid Monitoring of the Nature and Interconversion of Supported Catalyst Phases and of Their Influence Upon Performance: CO Oxidation to CO_2 by γ-Al_2O_3 Supported Rh Catalysts. *Chemistry–A European Journal* **2006**, *12*, 1975-1985.
32. Rui, W.; Xuebin, L.; Yanxin, C.; Wenzhao, L.; Hengyong, X. Effect of Metal–Support Interaction on Coking Resistance of Rh-Based Catalysts in CH_4/CO_2 Reforming. *Chinese Journal of Catalysis* **2007**, *28*, 865-869.
33. Vis, J.; Van't Buk, H.; Huizinga, T.; Van Grondelle, J.; Prins, R. Reduction and Oxidation of Rh/Al_2O_3 and Rh/TiO_2 Catalysts as Studied by Temperature-Programmed Reduction and Oxidation. *Journal of molecular catalysis* **1984**, *25*, 367-378.
34. Frenkel, A. I.; Hills, C. W.; Nuzzo, R. G. A view from the inside: complexity inthe atomic scale ordering of supported metal nanoparticles. *The Journal of Physical Chemistry B* **2001**, 105, 12689-12703.
35. Reimann, S.; StÒtzel, J.; Frahm, R.; Kleist, W.; Grunwaldt, J.-D.; Baiker, A. Identification of the Active Species Generated from Supported Pd Catalysts in Heck Reactions: An in Situ Quick Scanning Exafs Investigation. *Journal of the American Chemical Society* **2011**, *133*, 3921-3930.
36. Lu, Y.; Wang, J.; Yu, L.; Kovarik, L.; Zhang, X.; Hoffman, A. S.; Gallo, A.; Bare, S. R.; Sokaras, D.; Kroll, T. Identification of the Active Complex for CO Oxidation over Single-Atom Ir-on-$MgAl_2O_4$ Catalysts. *Nature Catalysis* **2019**, *2*, 149-156.
37. Wang, X.; Rodriguez, J.; Hanson, J.; Perez, M.; Evans, J. In Situ Time-Resolved Characterization of Au–CeO_2 and AuO_x–CeO_2 Catalysts During the Water-Gas Shift Reaction: Presence of Au and O Vacancies in the Active Phase. American Institute of Physics: 2005.

38. Wang, Q.; Hanson, J. C.; Frenkel, A. I. Solving the Structure of Reaction Intermediates by Time-Resolved Synchrotron X-Ray Absorption Spectroscopy. *The Journal of chemical physics* **2008**, *129*, 234502.
39. Yardimci, D.; Serna, P.; Gates, B. C. Tuning Catalytic Selectivity: Zeolite-and Magnesium Oxide-Supported Molecular Rhodium Catalysts for Hydrogenation of 1, 3-Butadiene. *Acs Catalysis* **2012**, *2*, 2100-2113.
40. Marks, L. Experimental Studies of Small Particle Structures. *Reports on Progress in Physics* **1994**, *57*, 603.
41. Frederick, R. T.; Diulus, J. T.; Hutchison, D. C.; Nyman, M.; Herman, G. S. Effect of Oxygen on Thermal and Radiation-Induced Chemistries in a Model Organotin Photoresist. *ACS applied materials & interfaces* **2019**, *11*, 4514-4522.
42. Davis, K. M.; Kosheleva, I.; Henning, R. W.; Seidler, G. T.; Pushkar, Y. Kinetic Modeling of the X-Ray-Induced Damage to a Metalloprotein. *The Journal of Physical Chemistry B* **2013**, *117*, 9161-9169.
43. Pagliero, A.; Mino, L.; Borfecchia, E.; Truccato, M.; Agostino, A.; Pascale, L.; Enrico, E.; Leo, N. D.; Lamberti, C.; Martínez-Criado, G. Doping Change in the Bi-2212 Superconductor Directly Induced by a Hard X-Ray Nanobeam. *Nano letters* **2014**, *14*, 1583-1589.
44. Wallander, H.; Wallentin, J. Simulated Sample Heating from a Nanofocused X-Ray Beam. *Journal of synchrotron radiation* **2017**, *24*, 925-933.
45. Hui, J.; Zhang, H.; Hu, Q.; Zhang, Z.; Ren, Y.; Zhang, L.; Wang, H. Investigation of Synchrotron X-Ray Induced Oxidation of Ag–Cu Thin-Film. *Materials Letters* **2020**, *272*, 127843.
46. Zerulla, D.; Chasse, T. X-Ray Induced Damage of Self-Assembled Alkanethiols on Gold and Indium Phosphide. *Langmuir* **1999**, *15*, 5285-5294.
47. Fuentes, S.; Figueras, F. The Influence of Particle Size on the Catalytic Properties of Alumina-Supported Rhodium Catalysts. *Journal of Catalysis* **1980**, *61*, 443-453.

TOC Graphic

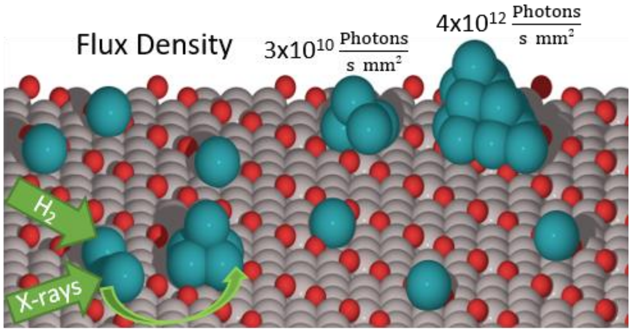
Flux Density
3x10^10 Photons / s mm^2
4x10^12 Photons / s mm^2
H2
X-rays